Enhanced nucleation and precipitation hardening in Al-Mg-Si(-Cu) alloys with minor Cd additions

Feng Qian[a,b], Dongdong Zhao[b], Eva A. Mørtsell[b], Shenbao Jin[c], Junsheng Wang[a], Calin D. Marioara[d], Sigmund J. Andersen[d], Gang Sha[c], Yanjun Li[b,*]

[a] School of Materials Science and Engineering, Beijing Institute of Technology, Beijing, 100081, China

[b] Department of Materials Science and Engineering, Norwegian University of Science and Technology, Trondheim, 7491, Norway

[c] School of Materials Science and Engineering, Herbert Gleiter Institute of Nanoscience, Nanjing University of Science and Technology, Nanjing, 210094, China

[d] SINTEF Materials and Nanotechnology, Trondheim, 7465, Norway

[*]Corresponding author. E-mail: yanjun.li@ntnu.no
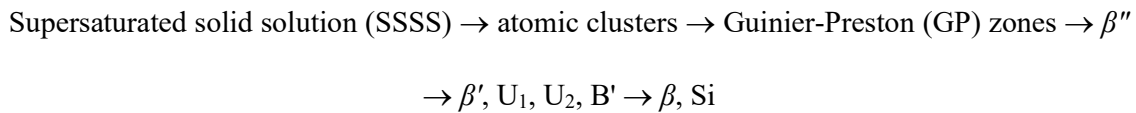
Abstract

This work reports a novel effect of impurity element Cd on enhancing the precipitation kinetics and increasing the peak hardness of Al-Mg-Si(-Cu) alloys during artificial ageing. It is found that the number density of age hardening Mg-Si(-Cu) precipitates is greatly increased by Cd addition (~0.06 at.%) at both the under-aged and peak-aged stages. A systematic study on the precipitation behaviour by high-angle annular dark-field scanning transmission electron microscopy (HAADF-STEM) shows that most Mg-Si(-Cu) precipitates in the Cd-containing Al-Mg-Si alloys are associated with Cd-rich precipitates and have highly disordered structures. It is also found that the formation of Q'/C-like sub-units in Mg-Si(-Cu) precipitates is significantly prompted by Cd additions. To explore the nucleation mechanism under the influence of Cd addition, atom probe tomography (APT) is applied to study the solute clustering behaviour in the early stages of artificial ageing, and density functional theory (DFT)

calculations are used to evaluate the binding energies of different solute-vacancy complexes and therefore the formation kinetics of Mg-Si-Cd clusters.

1   Introduction

6xxx Al-Mg-Si alloys are widely applied for structural purposes, such as in the automotive, aviation, marine and nuclear industries. As age-hardenable Al alloys, they are featured by a significant increase of hardness during artificial ageing (AA) at 160-200 °C [1–3] via the formation of a high density of nano-sized, (semi-)coherent, metastable precipitates [4]. The generic precipitation sequence of ternary Al-Mg-Si alloys is proposed as follows [5–20]:

Supersaturated solid solution (SSSS) $\rightarrow$ atomic clusters $\rightarrow$ Guinier-Preston (GP) zones $\rightarrow \beta''$

$$\rightarrow \beta', U_1, U_2, B' \rightarrow \beta, Si$$

Among these phases, β'' phase ($Si_4Mg_{5-x}Al_{2+x}$ (x=0, 1)) is the most effective strengthening phase in Al-Mg-Si alloys [2,9,10,12,13,20–26]. It has a needle shape with a C-centred monoclinic structure (C2/m, $a = 1.516$ nm, $b = 0.405$ nm, $c = 0.674$ nm, $\beta = 105.3°$, see Figure 1(a)) [2,12,13,27–29]. GP zones are also believed to have a contribution to the strength, but to a lesser extent [6,23]. Atomic clusters, as the precursors of GP zones and β'', set the initial conditions for the precipitation of the latter two phases in terms of composition and number density, and therefore plays a critical role for the age hardening response of alloys.
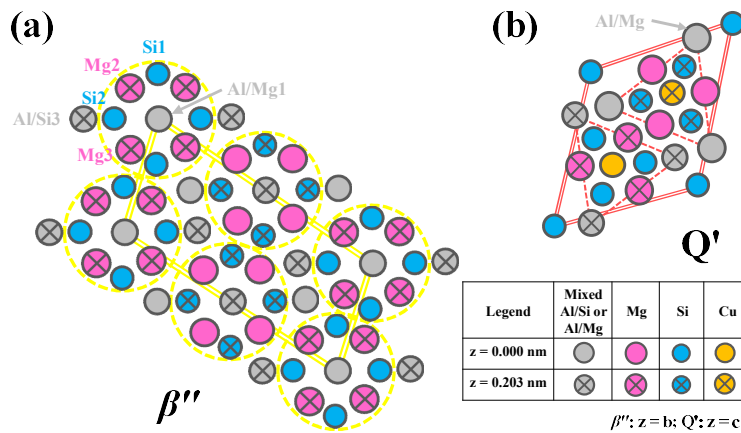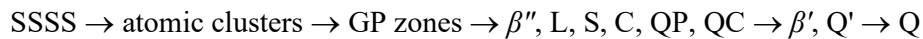

Figure 1 Schematic illustration of the unit cells of (a) β'' [2] and (b) Q' [30]. The characteristic eye-like sub-units in β'' are marked by yellow dashed circles; the characteristic triangular sub-units in Q' are marked by red dashed triangles.

A large number of studies have focused on manipulating the precipitation behaviour to increase the number density of β'' precipitates. Modifications of the heat treatment, such as pre-ageing [7,10,24,31–33] and interrupted quenching [34,35], have proved to be beneficial to the formation of effective atomic clusters for the later precipitation. Optimization of alloy compositions by decreasing Mg/Si ratios brought about a faster ageing response and a slower over-ageing response owing to a finer distribution of β'' precipitates [23,36–39]. There are also many studies about the effects of quaternary-element additions on the age hardening response of Al-Mg-Si alloys, such as Cu [39–48], Li [49,50], Ag [51–53], Ge [52,53] and Zn [54,55]. It has been demonstrated that the improved age hardening response of Al-Mg-Si alloys with quaternary-element additions are closely related to the modified precipitation sequences [42,49,52–56]. For example, additions of Cu to Al-Mg-Si alloys have been revealed to bring about significant changes in the precipitation sequence as follows [4,57]:

$$\text{SSSS} \rightarrow \text{atomic clusters} \rightarrow \text{GP zones} \rightarrow \beta'', \text{L, S, C, QP, QC} \rightarrow \beta', \text{Q'} \rightarrow \text{Q}$$

The addition of Cu suppresses the precipitation of β'' and prompts the formation of the quaternary phases, such as L, S, C, QP, QC, Q' and Q phase [4,14,42,44,46,56–58]. The metastable Q' phase is the coherent version of the equilibrium Q phase, and it has a lath shape with a hexagonal structure ($P\bar{6}$, $a = b = 1.032$ nm, $c = 0.405$ nm, $\gamma = 120°$) and a composition of $Al_xMg_{12-x}Cu_2Si_7$ (($3 \leq x \leq 6$)) [4,14,42,44,56,59], see Figure 1(b). For other quaternary-element additions, it was reported that Ge substitutes some of the Si sites in β'', which may be due to the similar electronic properties of Ge and Si [52,53]. Li preferentially occupies Mg3 sites in β'' [49]. Zn shows a weaker preference for certain atomic sites, and a partial occupancy on Al/Si3 sites was proposed [54,55]. Ag atoms are often observed at the incoherent precipitate/matrix interfaces or are incorporated into β' precipitates by replacing certain Si sites [51,60]. Recently, a new Q'/C-like triangular sub-unit containing Ag at the Cu sites was

reported [53]. In general, with the quaternary-element additions, precipitates with disordered structures will become more common.

Additions of impurity elements Cd, In and Sn have been reported to significantly increase the strength of Al-Cu alloys due to the refined dispersion of θ' [61–65]. However, the underlying mechanism is still controversial [61–71]. It was recently found that a trace amount of Sn in a 6061 alloy could retard natural ageing (NA) up to 2 weeks [1] and thus reduce the detrimental effect of NA on AA hardening response. Sn was suggested to possess optimal solute-vacancy bonding energies which can trap vacancies at RT and release them at AA temperatures [3,72–74]. In addition, it was also reported that Sn could improve the hardening response of Al-Mg-Si alloys at high ageing temperatures (>210 $^{\circ}$C) [3].

In a previous study, we reported that a minor addition of 0.06 at.% Cd in an Al-Mg-Si alloy can significantly accelerate the age hardening kinetics and give rise to an increase in peak hardness during ageing at 185 °C [75]. In this work, we find that when both Cd and Cu are added in an Al-Mg-Si alloy, the age hardening response can be further improved. The microstructural evolution of precipitates (including number density and size) in Cd-containing Al-Mg-Si(-Cu) alloys was quantitatively studied in comparison with their Cd-free counterparts. A detailed examination of the precipitate structures by high-angle annular dark-field scanning transmission electron microscopy (HAADF-STEM) has been carried out to clarify the effects of Cd on the precipitation sequences. More importantly, the clustering behaviour in the Cd-containing alloys during the early stages of AA has been studied by atom probe tomography (APT). Based on APT characterizations and density functional theory (DFT) calculations, the nucleation and precipitation mechanism of age-hardening precipitates under the influence of Cd addition was proposed.

2 Material and methods

Three experimental alloys with a similar Mg/Si ratio of ~0.6 and different levels of Cd and/or Cu content were prepared by remelting a commercial DC-cast 6082 alloy billet, adding pure Cu and/or Al-Cd master alloy and casting into a copper mould. The 6082 alloy was also investigated as a reference alloy. According to the difference of their Cu and Cd contents, the four experimental alloys are referred to as 6082, 6082Cu, 6082Cd and 6082CuCd alloys, respectively. The measured chemical compositions are given in Table 1.

Table 1 Measured chemical compositions (wt.% and at.%) of the experimental materials.

		Mn	Fe	Si	Mg	Cu	Cd	Al
6082	wt.%	0.50	0.20	1.12	0.55	0.01	-	bal.
	at.%	0.24	0.10	1.08	0.61	0.004	-	bal.
6082Cu	wt.%	0.49	0.18	1.08	0.56	0.27	-	bal.
	at.%	0.24	0.08	1.04	0.62	0.12	-	bal.
6082Cd	wt.%	0.52	0.21	1.06	0.50	0.01	0.24	bal.
	at.%	0.26	0.10	1.02	0.56	0.004	0.06	bal.
6082CuCd	wt.%	0.54	0.19	1.01	0.55	0.24	0.26	bal.
	at.%	0.26	0.09	0.98	0.62	0.10	0.06	bal.

Solution heat treatment (SHT) of the as-cast samples was carried out in an air furnace at 540 °C for 4 h followed by an immediate quenching into cold water. After a RT storage for 1 hour, AA at 185 °C for different times ranging from 5 min to 24 h was applied. Vickers hardness was measured by a Matsuzawa hardness tester under a 5 kg applied load and a dwell time of 15 s. Each data point in the hardness curves was based on an average of at least eight measurements. Ambient tensile testing was conducted on a CMT4105 tensile testing machine at an initial strain rate of 0.0007 s^{-1} with flat rectangular tensile specimens machined based on

ASTM standard (gauge length: 25 mm). An extensometer was used for the measurement of strain.

Thin foils for TEM studies were prepared with a standard mechanical polishing and electropolishing procedure described in Ref. [75]. A JEOL 2100 TEM equipped with electron energy loss spectroscopy (EELS) was employed for bright-field TEM observations. All the TEM images were taken along <100>$_{Al}$ zone axes. The number density (N_V), average length (λ), average cross-sectional area (φ) of elongated precipitates and average equivalent circular diameter ($\overline{D_s}$) of (near-)spherical precipitates were quantified. The number density of elongated precipitates is determined as $N_V = \frac{3N}{A(\lambda+t)}$, where N is the counted number of precipitate cross-sections in the viewing direction within the area (A) of the image and t is the thickness of TEM foil estimated by EELS. The number density of (near-)spherical precipitates is determined as $N_V = \frac{N}{A(\overline{D_s}+t)}$. At least six sample areas/images and more than 150 precipitates were analysed for each sample. A more detailed description of the method for precipitate quantification can be found elsewhere [23,76,77]. HAADF-STEM images were recorded by using a double aberration-corrected (image and probe Cs) cold-FEG JEOL ARM-200F operated at 200 kV, with a probe size of 0.08 nm, a convergence semi-angle of 28 mrad and an inner collection angle of 35 mrad. This microscope is equipped with a Gatan Imaging Filter (GIF) Quantum spectrometer which enables the acquisition of EELS elemental maps. Electron energy loss spectra were obtained in the energy loss range 300-1324 eV, which includes the energy loss edges Cd-$M_{4,5}$ at 404 eV, Cu-L_1 at 1096 eV and Cu-L_2 at 951 eV. The manual integration of EELS edges was performed after power-law background subtraction.

Needle-shaped APT samples were prepared by etching small square rods ($0.5 \times 0.5 \times 15$ mm^3) with a two-step electropolishing method described in Ref. [77]. The APT characterization was

performed on a local electrode atom probe LEAP4000X SI under a high vacuum of 2×10^{-9} Pa, at a sample temperature of 20 K, a UV laser pulsing energy of 40 pJ, a repetition rate of 250 kHz and a target evaporation rate of 0.5%. Data reconstruction and statistical analyses were conducted by using Cameca IVAS 3.6.12 software, where the reconstruction parameters are refined based on the crystalline patterns from desorption maps during APT running. The maximum separation algorithm [78] was employed for cluster identification by using Cd, Mg and Si as target elements. The maximum separation distance between the solute atoms in one cluster, d_{max}, is set as 0.6 nm and the minimum number of solute atoms in one cluster, N_{min}, is set as 7.

DFT calculations in the present work were carried out using the Vienna ab initio simulation package (VASP), which adopted the frozen-core Projector Augmented Wave method [79][80] to depict the electron-ion interactions, and the Generalized Gradient Approximation (GGA) of Perdew-Burke-Ernzerhof (PBE) [81] to describe the exchange-correlation. Plane wave cut-off energy was set to be 400 eV in all the calculations. The Monkhorst-Pack scheme [82] k-points sampling in combination with the linear tetrahedron method including Blöchl corrections [83] were utilized for the total energy integrations of the Brillouin zone (BZ). Supercells containing 108 atoms (based on $3 \times 3 \times 3$ unit cells of Al) were constructed to calculate the binding energy between different solute atoms and vacancies (Va) including Cd-Si-Va, Cd-Mg-Va, Mg-Si-Va in the Al matrix. Within the supercell, the substitutional impurities and vacancies were set as 1st nearest neighbours in between each other. Each complex has seven different potential geometries as a result of the different arrangements of impurities and vacancies (straight or triangle arrangements as indicated in Table 2). Full relaxations in respect to volume, the shape of the cell, and the atomic positions were implemented until the Hellmann-Feynman force on

all atoms was $< 10^{-2}$ eV·Å^{-1}. The binding energy of the complexes was determined by the following equation [84][85]:

$$E_{X-Y-V}^{Bind} = -\left(E_{Al_{105}XYVa}^{tot} - E_{Al_{107}X}^{tot} - E_{Al_{107}Y}^{tot} - E_{Al_{107}Va}^{tot} + 2 \cdot E_{Al_{108}}^{tot}\right), \quad X,Y = Cd, Mg, Si$$

Eq. (1)

where $E_{Al_{105}XYVa}^{tot}$ is the total calculated energy of the supercell containing a X-Y-Va complex, while $E_{Al_{107}X}^{tot}$, $E_{Al_{107}Y}^{tot}$, $E_{Al_{107}Va}^{tot}$ stand for the total energy of the supercell containing a single solute atom X, Y or a vacancy, respectively. $E_{Al_{108}}^{tot}$ represents the total energy of the supercell having 108 Al atoms.

3   Results

3.1   Age hardening response

3.1.1   Vickers hardness evolution

The Vickers hardness evolution of the four experimental alloys during AA at 185 °C is presented in Figure 2. Before AA, the four alloys have similar hardnesses in the range of 45~50 HV. During AA, both the 6082Cu and 6082Cd alloys exhibit accelerated age-hardening kinetics in comparison to the 6082 base alloy, but the hardening kinetics of the 6082Cd alloy (92 HV after 30 min ageing) is even faster than that of the 6082Cu alloy (80 HV after 30 min ageing). Moreover, the peak hardness of the 6082Cd alloy (124 HV) is moderately increased compared to the 6082 base alloy (116 HV), while no difference in peak hardness is detected in the 6082Cu alloy. Adding both Cu and Cd leads to a further improved age-hardening response: the 6082CuCd alloy achieves a hardness of 98 HV after 30 min ageing and a further increase of peak hardness to 131 HV within 120 min ageing.
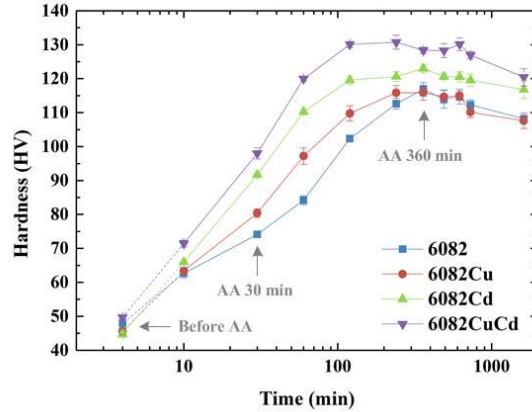
Figure 2 Vickers hardness evolution of the 6082, 6082Cu, 6082Cd and 6082CuCd alloys during ageing at 185 °C.

3.1.2 Bright-field TEM observation of precipitates

The bright-field TEM micrographs of precipitates in the four alloys aged at 185 °C for 30 min and 360 min are illustrated in Figure 3(a) and (b), respectively. Fine, dark dot-shaped contrasts, which correspond to the cross-sections of precipitates (in the $\langle 100 \rangle_{Al}$ viewing direction), can be observed in the four alloys, but the Cd-containing alloys show a much-refined precipitate microstructure compared to the Cd-free alloys at both AA stages (30 min and 360 min). It is worth noting that, after 360 min ageing, lath-shaped Q' precipitates, which can be identified by their elongated cross-sections align in $\langle 510 \rangle_{Al}$ directions, are frequently observed in the 6082CuCd alloy (indicated by red arrows in Figure 3(b)); while in the 6082Cu alloy, well-developed Q' precipitate is barely noticed.

The quantitative measurement of elongated Mg-Si(-Cu) precipitates (including needle-shaped β'', lath-shaped Q' and their precursors) in the four alloys were conducted based on bright-field TEM and HAADF-STEM observations, and the average number densities of precipitates are representatively shown in Figure 3(c). Our previous work [75] has demonstrated that the dark-dot contrasts observed in bright-field TEM images (Figure 3(a) and (b)) correspond to three types of precipitates: single Mg-Si(-Cu) precipitates, single Cd-rich precipitates and

10

"composite" precipitates containing the former two precipitates. Therefore, the population proportions of the three types of precipitates were determined by HAADF-STEM analyses, which provides a more accurate number density of Mg-Si(-Cu) precipitates. As shown in Figure 3(c), Cd-containing Al-Mg-Si alloys have much higher number densities of precipitates than their Cd-free counterparts. For example, after 30 min ageing, the number densities of precipitates in the 6082Cd and 6082CuCd alloys are 6.4 and 2.1 times as high as the 6082 alloy and 6082Cu alloys, respectively. It is worth noting that, although after ageing for 360 min, the number density of precipitates in the 6082CuCd alloy was decreased due to over ageing, it is still much higher than that of the 6082 base and 6082Cu alloys.
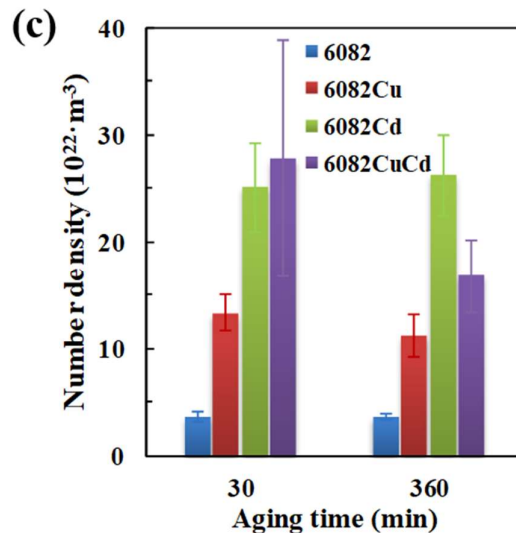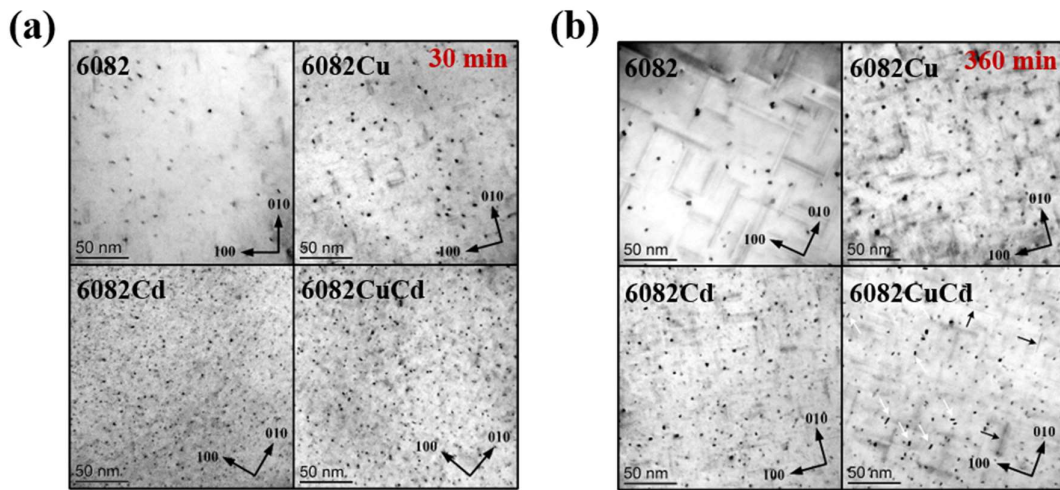
Figure 3 Bright-field TEM micrographs of the 6082, 6082Cu, 6082Cd and 6082CuCd alloys aged at 185 °C for (a)30 min, the corresponding foil thicknesses were measured as 70 nm, 46 nm, 42 nm and 49 nm, respectively; (b) 360 min, the corresponding foil thicknesses were measured as 50 nm, 52 nm, 36 nm and 71 nm, respectively, the white arrows point lath-shaped Q′ precipitates with elongated cross-sections along <510>$_{Al}$ direction while the black arrows point the possible plate-shaped C precipitates; (c) number densities of elongated Mg-Si(-Cu) precipitates in the four alloys aged for 30 and 360 min.

3.2   HAADF-STEM characterization of precipitates

3.2.1   Precipitates in the 6082Cd alloy

The atomic structure of precipitates in the aged 6082 and 6082Cd alloys has been shown in Ref. [75]. It reveals that many of the precipitates in the 6082Cd alloy have a "composite" structure consisting of one Cd-rich precipitate and one needle-shaped β'' precipitate or the precursor of β'' associated with it. Another interesting finding about the 6082Cd alloy is that Q′/C-like sub-units (Figure 1(b)) are observed in some of the needle-shaped precipitates attached to Cd-rich precipitates.

Therefore, HAADF-STEM-EELS analyses were conducted to identify the composition of the Q′/C-like sub-units in the 6082Cd alloy. Figure 4(a) shows the HAADF-STEM micrograph of a typical "composite" precipitate formed after ageing at 185 °C for 360 min. The rectangular Cd-rich precipitate (marked by a green box) seems to have a periodic ordering, and the attached needle-shaped precipitate contains several Q′/C-like sub-units (indicated by red dashed triangles). The corresponding EELS elemental maps of Cd and Cu are presented in Figure 4(b) and (c, d), respectively. The Cd-rich precipitate with bright contrast in Figure 4(a) is indicated in the Cd map by a green box in Figure 4(b). It is worth noting that strong Cu signals are also detected within the Cd-rich precipitate (Figure 4(c) and (d)). For the needle-shaped precipitate, Cu signals are also detected, but Cd is almost absent in this region. Most importantly, several intensity peaks in the Cu maps (pointed by red arrows) correspond well with the central sites of Q′/C-like sub-units in Figure 4(a), confirming that the central sites of such sub-units observed in the 6082Cd alloy aged for 360 min are occupied by Cu atoms. These Cu-centred Q′/C-like sub-units are frequently observed in Al-Mg-Si-Cu alloys with Cu contents higher
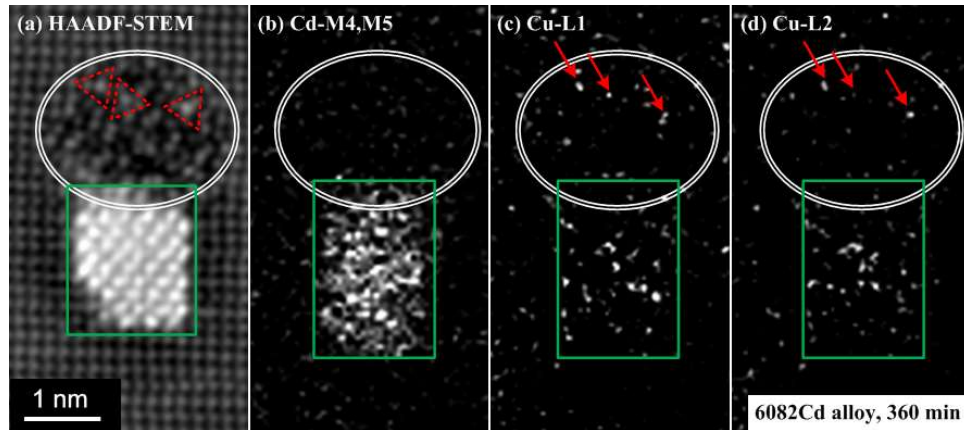
Figure 4 (a) HAADF-STEM micrograph of a "composite" precipitate in the 6082Cd alloy aged at 185 °C for 360 min taken before the EELS scan. The Q'/C-like sub-units in the needle-shaped precipitate are indicated by red dashed triangles. EELS elemental maps of (b) Cd and (c, d) Cu. The elongation of the Cd-rich region in the vertical direction in (b)-(d) compared to (a) is due to a slight drift of sample during EELS scan.

3.2.2 Precipitates in the 6082CuCd alloy

Figure 5 displays a series of HAADF-STEM images of the precipitates in the 6082CuCd alloy aged at 185 °C for different times. After 30 min ageing, small "composite" precipitates consisting of a tiny Cd-rich region surrounded by several eye-like sub-units (labelled by yellow circles) of β'' precipitate can be observed (Figure 5(a)). In some "composite" precipitates, Q'/C-like triangular sub-units and even complete Q' unit cells have already formed (Figure 5(b)). After 360 min ageing, "composite" precipitates have grown to larger sizes. In addition to needle-shaped precipitates with highly disordered cross-section structure (Figure 5(c)), well-developed lath-shaped Q' precipitates are found to be attached to Cd-rich precipitates (Figure 5(d)). It is interesting to see that there are several atomic columns with bright contrasts at the Q'/Al interface, which have a six-fold symmetry with the atomic columns with bright contrast in the Q' precipitate.
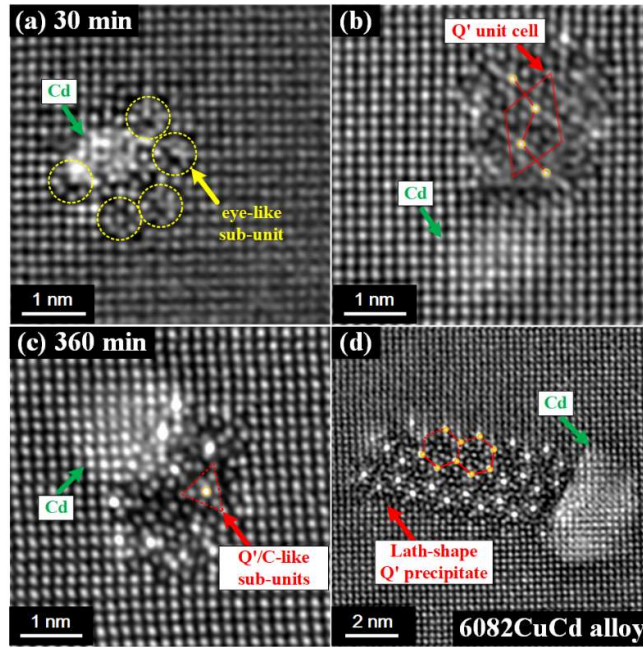
13

Figure 5 HAADF-STEM micrographs of precipitates in the 6082CuCd alloy aged at 185 °C for (a, b) 30 min and (c, d) 360 min, respectively.

3.3 APT characterization of atomic clusters and precipitates

To investigate the influence of Cd addition on the atomic clustering behaviour, an APT study was carried out on the 6082CuCd alloy aged at 185 °C for 5 min. Three-dimensional atom maps of Cd (green), Mg (magenta), Si (blue) and Cu (orange) are shown in Figure 6(a). No precipitate but a high density of Cd-rich clusters have formed. Nearest neighbour distribution (NND) analyses (Figure 6(b)) further reveal that, in addition to Cd clustering, the clustering of Mg and Si atoms have also initiated, but Cu atoms are still distributed randomly within the matrix. Figure 6(c) shows the distribution of clusters which were identified by using Cd, Mg and Si as target elements. The number density of clusters is determined as 3.2×10^{24} m^{-3}. A statistical analysis of all 336 Mg-Si(-Cd) clusters in the selected volume reveals that most of the Mg-Si-Cd clusters have a larger size than Cd-free Mg-Si clusters: 44.4% of Mg-Si-Cd clusters consist of ≥ 10 solute atoms, whereas only 17.2% of Cd-free Mg-Si clusters have ≥ 10

14

solute atoms (Figure 6(d)). In addition, about 73% of Mg-Si-Cd clusters have a Mg/Si ratio $\geq$ 1, while only about 56% of Mg-Si clusters have a Mg/Si ratio $\geq$ 1.
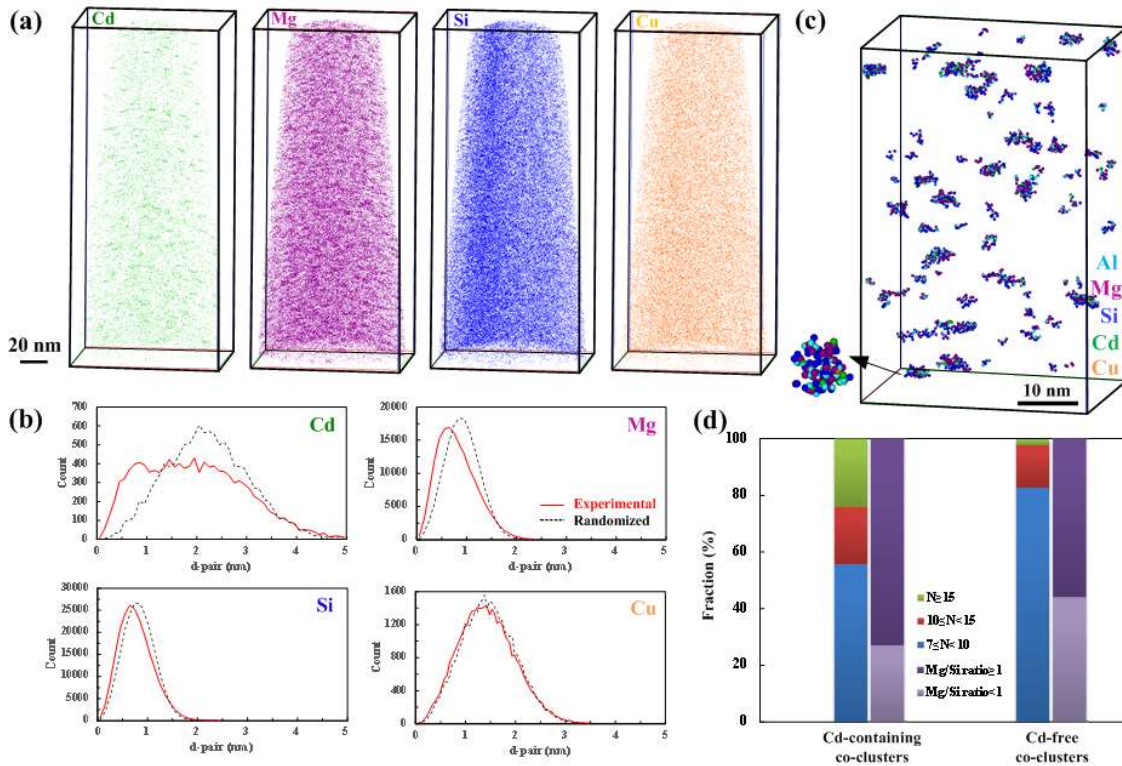

Figure 6 APT results of the 6082CuCd alloy aged at 185 °C for 5 min. (a) three-dimensional atom maps of Cd (green), Mg (magenta), Si (blue) and Cu (orange) within the selected volume; (b) nearest neighbour distribution data of Cd, Mg, Si and Cu atoms; (c) distribution of clusters identified by target elements: Mg, Si and Cd; (d) the fraction of cluster size (N: number of solute atoms in clusters) and Mg/Si ratio of both Cd-containing and Cd-free clusters..

Figure 7 presents results of the APT study on the 6082CuCd alloy aged at 185 °C for 60 min. The non-uniform distribution of Cd, Mg, Si, as well as Cu but to a lesser extent, can be clearly seen in the atom maps in Figure 7(a). The 0.8 at.% Cd concentration and 3.2 at.% Mg concentration isosurfaces are used to visualize the Cd-rich and Mg-Si(-Cu) precipitates, respectively (see Figure 7(b)). High number densities of near-spherical Cd-rich precipitates and elongated Mg-Si(-Cu) precipitates are visible after 60 min ageing. A closer observation of these precipitates reveals that most of the Mg-Si(-Cu) precipitates are associated with Cd-rich precipitates at either end of the precipitates, which agrees well with HAADF-STEM observations (Figure 4 and 5). In Figure 7(c), the proximity histograms (proxigrams) of several

Cd-rich precipitates show that the Cd-rich precipitates contain a considerable amount of Mg and Si as well as a trace level of Cu, even in the centre of Cd-rich precipitates, which is consistent with EELS analyses (Figure 4). While within the Mg-Si-Cu precipitates, the concentration peak of Cd is also detected, indicating that the precipitates contain a trace level of Cd.
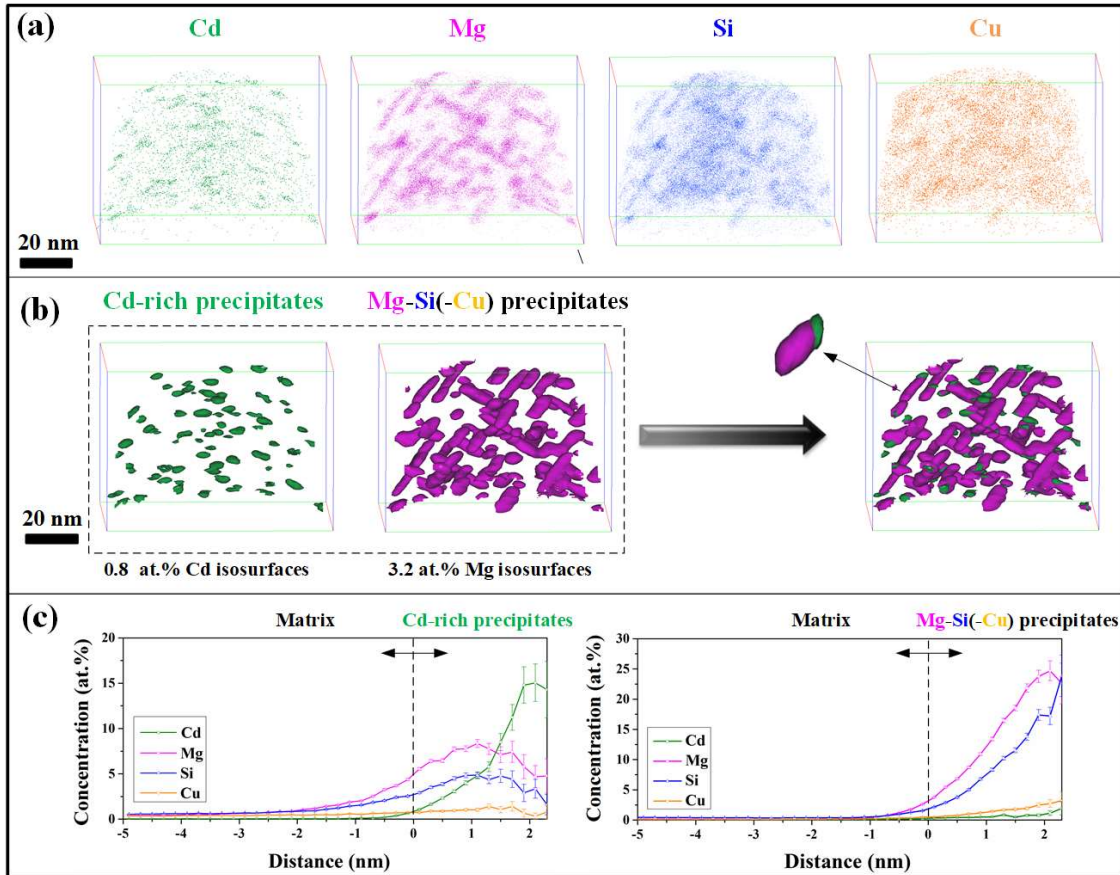

Figure 7 APT results of the 6082CuCd alloy aged at 185 °C for 60 min. (a) Atom maps of Cd (green), Mg (magenta), Si (blue) and Cu (orange) within the selected volume; (b) isosurfaces (green) for regions with higher than 0.8 at.% Cd and isosurfaces (magenta) for regions with higher than 3.2 at.% Mg; (c) proximity histograms of Cd-rich precipitates and Mg-Si(-Cu) precipitates, respectively.

3.4 Tensile properties

The results of tensile testing on the four alloys aged at 185 °C for 30, 120 and 360 min is presented in Figure 8. In agreement with the hardness curves (Figure 1), both yield strength (YS) and ultimate tensile strength (UTS) of Cd-containing alloys are higher than those of Cd-

free alloys at every AA stage. After 30 min ageing, the YS of 6082Cd and 6082CuCd alloys have reached 216 ± 3 and 219 ± 2 MPa, respectively, while the YS of both 6082 and 6082Cu alloys are less than 160 Mpa (Figure 8(a)). Even after 360 min ageing, the YS of the 6082Cd and 6082CuCd alloys are still higher than Cd-free alloys.
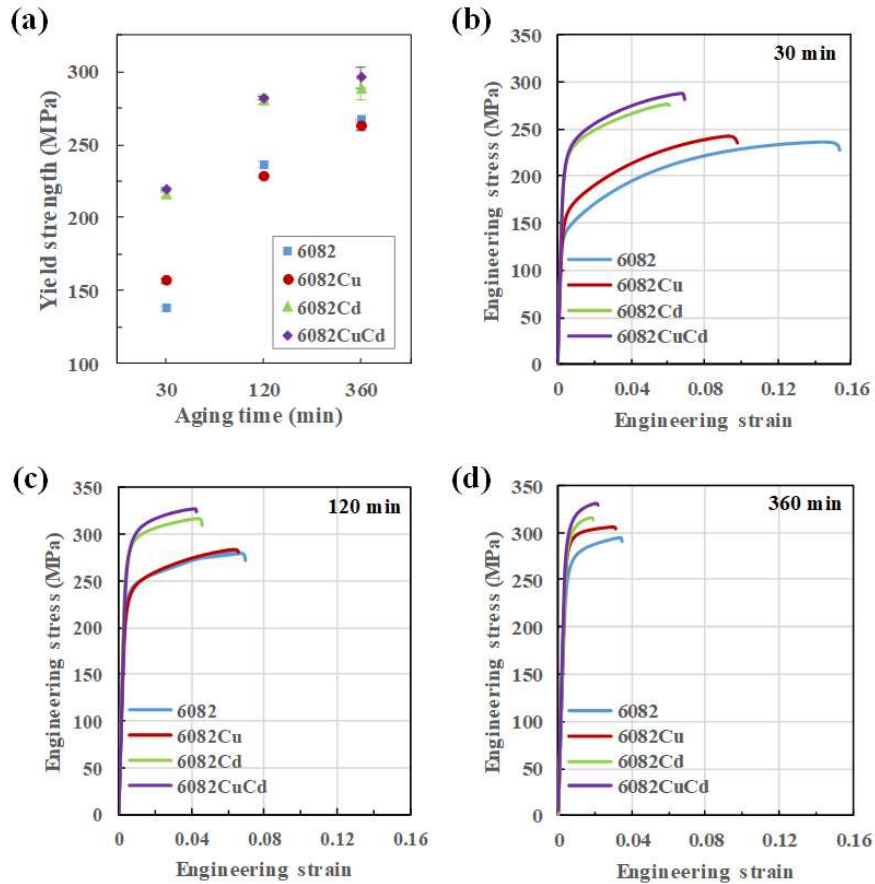

Figure 8 (a) YS of the four alloys aged at 185 °C for 30, 120 and 360 min; engineering stress-strain curves of the four alloys aged for (b) 30 min, (c) 120 min and (d) 360 min, respectively.

4   Discussion

4.1   The effect of Cd on precipitate nucleation in Al-Mg-Si alloys

The nucleation of age-hardening precipitates is known to start from the decomposition of the supersaturated solid solution and the formation of solute clusters via vacancy-aided solute
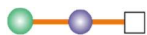
17
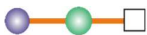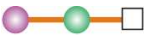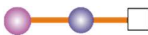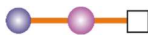
diffusion. In Al-Mg-Si alloys, since Si has a lower solubility and a higher diffusivity than Mg in the Al matrix [86], clustering of Si atoms is likely to occur first, followed by the diffusion of Mg atoms towards Si clusters to form Mg-Si clusters [20,36,87]. This means the Mg/Si ratio of individual clusters at the initial stages of clustering can largely vary [7,10,21,23,31,36,37,41,88–90], and it is widely accepted that the cluster with a Mg/Si ratio close to that of GP zones or β'', i.e. ~1 or slightly higher, can transform to or act as nuclei for the strengthening phases more easily [7,10,20,36,87,90,91].
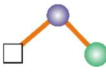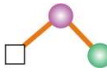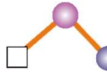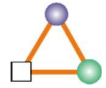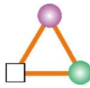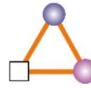
In microalloyed Al-Mg-Si alloys, the mechanisms for the nucleation of precipitates can be modified with different quaternary-element additions [46,53,92]. For Al-Mg-Si alloys with Cu additions, Zandbergen et al. [46] suggested that the substitution of Mg by Cu in clusters reduces the strain energy and is beneficial to the later growth of clusters and their transformation into precipitates. In the case of Ge-containing Al-Mg-Si alloys, it was proposed that the high affinity of Ge with vacancies enables Ge to create nucleation sites for β'' [53]. Recently, it was reported that the suppressed annihilation of quenched-in vacancies by Sn is the main reason for the fast ageing kinetics of Al-Mg-Si alloys at unconventional ageing temperatures (>210 $^{\circ}$C) [3]. A recent study further suggested that the enhanced nucleation of precipitates in Sn-containing Al-Mg-Si alloys during ageing at 250 °C is related to the formation of β' phase ($Mg_9Si_{5-x}Sn_x$) on Sn-vacancy complexes [92].

In the present Cd-containing Al-Mg-Si alloys, APT analyses suggested that the clustering process is significantly modified by Cd additions, and the mechanism for the enhanced nucleation of precipitates in Al-Mg-Si alloys by Cd addition seems to be different from those mentioned above. Previous DFT calculation results by Wolverton [93] show that the binding energy of Cd-Va complexes is 0.14 eV, which is much higher than Mg-Va (-0.02 eV) and Si-Va (0.08 eV) complexes. In this study, the binding energies of ternary complexes including

two different solute atoms and one vacancy with all possible arrangements in the Al matrix are calculated via the DFT method. As shown in Table 2, the binding energies of Cd-Mg-Va complexes with all arrangements and Cd-Si-Va complexes with most arrangements are higher than that of Mg-Va and Si-Va pairs, respectively, and in some cases are even higher than Cd-Va pairs. Besides, the binding energies of Cd-Mg-Va and Cd-Si-Va complexes with most arrangements are also higher than the Mg-Si-Va complexes. It suggests that the Cd-Mg-Va and Cd-Si-Va complexes are energetically more favourable than Mg-Va, Si-Va and Mg-Si-Va pairs/complexes. Although the binding energies of Mg-Si-Cd-Va complexes are not calculated, it can be speculated that they also have high binding energies. Therefore, the modified clustering process is proposed to take place by the formation of Cd-Mg-Va and Cd-Si-Va complexes, and the aggregation of them consequently produces Mg-Si-Cd-Va clusters. This is consistent with our APT observations on the 6082CuCd alloy showing that a high density of Mg-Si-Cd clusters were formed after 5 mins AA (Figure 6).

Table 2 Different straight and triangle arrangements of Cd-Si-Va, Cd-Mg-Va, Mg-Si-Va complexes in the Al matrix and the corresponding binding energy (eV) as determined by DFT calculations. In the complexes, ● stands for Cd atoms, and ● for Mg, ● for Si, □ for vacancies, respectively.

Cd-Si-Va complexes	Binding energy (eV)	Cd-Mg-Va complexes	Binding energy (eV)	Mg-Si-Va complexes	Binding energy (eV)
●—●—□	0.148	●—●—□	0.193	●—●—□	0.118
●—●—□	0.042	●—●—□	0.047	●—●—□	0.010
●—□—●	0.217	●—□—●	0.126	●—□—●	0.048
triangle	0.209	triangle	0.152	triangle	0.033
triangle	0.139	triangle	0.200	triangle	0.088

	0.013		0.016		0.023
	0.197		0.174		0.116

Based on the proposed clustering process, the effects of Cd on the clustering process are discussed. First, the high binding energies of Cd-Va, Cd-Mg-Va and Cd-Si-Va pairs/complexes can increase the equilibrium concentration of vacancies at SHT temperatures and stabilize the quenched-in vacancies during RT storage for the clustering process in the later AA stages. Besides, the high binding energies of Cd-Mg-Va and Cd-Si-Va complexes is considered to enhance the interaction between solute atoms (mainly Mg and Si) and vacancies, which further accelerates the diffusion of solute atoms and thus the clustering process. As a result, the Mg-Si-Cd clusters are more likely to grow to larger sizes compared to Mg-Si clusters (Figure 6(d)). It is worth noting that the binding energies of Cd-Mg-Va complexes are much higher than Mg-Va and Mg-Si-Va pairs/complexes and are comparable to Cd-Si-Va complexes (Table 2). Such high binding energies can significantly accelerate the diffusion of Mg atoms, favouring the formation of Mg-Si-Cd clusters with higher Mg/Si ratios (indicated by APT analyses shown in Figure 6(d)) which can transform to or act as nuclei for β'' more easily during the later stages of AA [7,37,87].

4.2   The effect of Cd on precipitation sequence in Al-Mg-Si alloys

In addition to the positive effect on the nucleation of Mg-Si(-Cu) precipitates, Cd is also found to alter the precipitation sequence in Al-Mg-Si alloys. In addition to Mg-Si(-Cu) precipitates, Cd-rich precipitates also formed during artificial ageing, mostly attached to Mg-Si(-Cu) precipitates, showing as "composite" precipitates, and occasionally as single precipitates. The

20

"composite" structure of precipitates observed in the present Cd-containing alloys has never been reported in Al-Mg-Si alloys with additions of other alloying elements, such as Cu, Ge, Li, Zn, Ag and Sn [30,52,54,60,92]. These elements are generally found to be incorporated into β''/β' precipitates by either occupying certain atomic sites, forming new local configurations (e.g. Q'/C-like sub-units) or new precipitates (e.g. Q' phase with the addition of Cu). In contrast, most Cd atoms in Al-Mg-Si alloys exist in the form of Cd-rich precipitates associated with Mg-Si(-Cu) precipitates and the trace amount of Cd atoms in Mg-Si(-Cu) precipitates show no preference for particular atomic sites (Figure 4 and 5). The trace amount of Cd atoms is also believed to be responsible for the highly disordered structure of Mg-Si(-Cu) precipitates in Cd-containing alloys.

Besides, the presence of "composite" precipitates is considered as evidence for the nucleation of Mg-Si(-Cu) precipitates on Mg-Si-Cd clusters. During the nucleation and later growth of precipitates, Cd atoms were gradually rejected probably due to a lower solubility in Mg-Si(-Cu) precipitates, forming Al-Cd clusters/precipitates attached to Al-Mg-Si(-Cu) precipitates. The trace level of Mg and Si in Cd-rich precipitates and that of Cd in Mg-Si(-Cu) precipitates (Figure 7(c)) is considered to be due to an incomplete rejection, which in turn confirms the separation process between Mg-Si(-Cu) precipitates and Al-Cd precipitates.

Another interesting finding is that the Cd addition prompts the formation of Q'/C-like sub-units in Mg-Si(-Cu) precipitates as well as the formation of Q' precipitates in Al-Mg-Si(-Cu) alloys. In the 6082Cd alloy, a large number of needle-shaped Mg-Si precipitates attached to Cd-rich precipitates formed after ageing for 360 min contain Q'/C-like sub-units and the central sites of these sub-units are indeed occupied by Cu (Figure 4), which is unexpected in an alloy with such a low Cu content of 0.01 wt.%. This effect is even stronger when the Cu content of the alloy is increased. In the 6082CuCd alloy, Q'/C-like sub-units and even complete Q' unit cells

have already formed in "composite" precipitates after ageing at 185 °C for only 30 min (Figure 5(b)). After ageing for 360 min, about 11% of the Mg-Si(-Cu) precipitates are identified as Q' phase (Figure 3(b)). In contrast, the fraction of Q' precipitates in the 6082Cu alloy is less than 1 %. Our APT analyses on the 6082CuCd alloy show that the distribution of Cu atoms was uniform after ageing for 5 min (Figure 6), which indicates that Cu did not participate in the initial clustering process. This is reasonable if considering that Cu has a higher solubility [94] and a lower diffusivity [86] than Mg, Si and Cd in Al at 185 °C. In the later stages of precipitation, Cu atoms are found to partition into Al-Cd clusters/precipitates (Figure 4 and Figure 7(c)), which is probably due to the relatively high binding energies of Cd-Cu-Va complexes [95]. These Cd-rich clusters/precipitates are supposed to provide Cu atoms for the formation of Q'/C-like sub-units in attached Mg-Si(-Cu) precipitates and Q' precipitates. The enhanced incorporation of Cu aided by Cd is also considered as another reason for the highly disordered structure of Mg-Si(-Cu) precipitates in Cd-containing alloys.

5   Conclusions

1. Minor addition of Cd (0.06 at.%) in an Al-Mg-Si alloy leads to accelerated hardening kinetics as well as an increase in peak hardness during ageing at 185 °C. The yield strengths after ageing for 30 min is increased by 57% with Cd addition. This effect is more significant when both Cd and Cu are added in the alloy.

2. The Cd addition substantially stimulates the nucleation of precipitates and therefore leads to a much-refined precipitate microstructure in Al-Mg-Si(-Cu) alloys. After ageing for 30 min, the number densities of Mg-Si(-Cu) strengthening precipitates in Cd-containing alloys are at least two times as high as their Cd-free counterparts.

3. Most of the Mg-Si(-Cu) precipitates formed in Cd-containing alloys are found to be associated with Cd-rich precipitates and highly disordered. Besides, the formation of Q'/C-like sub-units in Mg-Si(-Cu) precipitates is substantially prompted due to Cd additions.

4. With Cd addition, a high density of Mg-Si-Cd clusters is formed in the very early stages of AA. APT analyses show that most Mg-Si-Cd clusters have larger sizes and higher Mg/Si ratios than Mg-Si clusters, which can transform to or act as nuclei for the strengthening phases more easily.

5. The higher binding energies of Cd-Si-Va and Cd-Mg-Va complexes than Mg-Si-Va complexes obtained by DFT calculations are suggested to prompt the formation of Mg-Si-Cd-Va clusters and the later nucleation of Mg-Si(-Cu) precipitates, both thermodynamically and kinetically.

Acknowledgements

References

[1]   S. Pogatscher, H. Antrekowitsch, M. Werinos, F. Moszner, S.S.A. Gerstl, M.F. Francis, W.A. Curtin, J.F. Löffler, P.J. Uggowitzer, Diffusion on Demand to Control Precipitation Aging: Application to Al-Mg-Si Alloys, Phys. Rev. Lett. 112 (2014) 225701. https://doi.org/10.1103/PhysRevLett.112.225701.

[2]   P.H. Ninive, A. Strandlie, S. Gulbrandsen-Dahl, W. Lefebvre, C.D. Marioara, S.J. Andersen, J. Friis, R. Holmestad, O.M. Løvvik, Detailed atomistic insight into the β'' phase in Al–Mg–Si alloys, Acta Mater. 69 (2014) 126–134. https://doi.org/10.1016/j.actamat.2014.01.052.

[3]   M. Werinos, H. Antrekowitsch, E. Kozeschnik, T. Ebner, F. Moszner, J.F. Löffler, P.J. Uggowitzer, S. Pogatscher, Ultrafast artificial aging of Al–Mg–Si alloys, Scr. Mater. 112 (2016) 148–151. https://doi.org/10.1016/j.scriptamat.2015.09.037.

[4]   C.D. Marioara, S.J. Andersen, T.N. Stene, H. Hasting, J. Walmsley, A.T.J. Van Helvoort, R. Holmestad, The effect of Cu on precipitation in Al–Mg–Si alloys, Philos. Mag. 87 (2007) 3385–3413. https://doi.org/10.1080/14786430701287377.

[5]   J.H. Chen, E. Costan, M.A. van Huis, Q. Xu, H.W. Zandbergen, Atomic pillar-based nanoprecipitates strengthen AlMgSi alloys, Science. 312 (2006) 416–9. https://doi.org/10.1126/science.1124199.

[6]   C.D. Marioara, S.J. Andersen, J. Jansen, H.W. Zandbergen, Atomic model for GP-zones in a 6082 Al–Mg–Si system, Acta Mater. 49 (2001) 321–328. https://doi.org/10.1016/S1359-6454(00)00302-5.

[7]   M.W. Zandbergen, Q. Xu, A. Cerezo, G.D.W. Smith, Study of precipitation in Al–Mg–Si alloys by Atom Probe Tomography I. Microstructural changes as a function of ageing temperature, Acta Mater. 101 (2015) 136–148. https://doi.org/10.1016/j.actamat.2015.08.017.

[8]   D. Zhao, L. Zhou, Y. Kong, A. Wang, J. Wang, Y. Peng, Y. Du, Y. Ouyang, W. Zhang, Structure and thermodynamics of the key precipitated phases in the Al--Mg--Si alloys from first-principles calculations, J. Mater. Sci. 46 (2011) 7839. https://doi.org/10.1007/s10853-011-5765-4.

[9]   M.A. van Huis, J.H. Chen, H.W. Zandbergen, M.H.F. Sluiter, Phase stability and structural relations of nanometer-sized, matrix-embedded precipitate phases in Al–Mg–Si alloys in the late stages of evolution, Acta Mater. 54 (2006) 2945–2955. https://doi.org/https://doi.org/10.1016/j.actamat.2006.02.034.

[10]   M. Torsæter, H.S. Hasting, W. Lefebvre, C.D. Marioara, J.C. Walmsley, S.J. Andersen, R. Holmestad, The influence of composition and natural aging on clustering during preaging in Al–Mg–Si alloys, J. Appl. Phys. 108 (2010) 073527. https://doi.org/10.1063/1.3481090.

[11]   S.D. Dumolt, D.E. Laughlin, J.C. Williams, Formation of a modified β' phase in aluminum alloy 6061, Scr. Metall. 18 (1984) 1347–1350. https://doi.org/https://doi.org/10.1016/0036-9748(84)90362-4.

[12]   H.W. Zandbergen, S.J. Andersen, J. Jansen, Structure Determination of Mg5Si6 Particles in Al by Dynamic Electron Diffraction Studies, Science (80-.). 277 (1997) 1221–1225. http://science.sciencemag.org/content/277/5330/1221.abstract.

[13] S.J. Andersen, H.W. Zandbergen, J. Jansen, C. TrÆholt, U. Tundal, O. Reiso, The crystal structure of the β″ phase in Al–Mg–Si alloys, Acta Mater. 46 (1998) 3283–3298. https://doi.org/10.1016/S1359-6454(97)00493-X.

[14] C. Ravi, C. Wolverton, First-principles study of crystal structure and stability of Al–Mg–Si–(Cu) precipitates, Acta Mater. 52 (2004) 4213–4227. https://doi.org/https://doi.org/10.1016/j.actamat.2004.05.037.

[15] R. Vissers, M.A. van Huis, J. Jansen, H.W. Zandbergen, C.D. Marioara, S.J. Andersen, The crystal structure of the β′ phase in Al–Mg–Si alloys, Acta Mater. 55 (2007) 3815–3823. https://doi.org/10.1016/j.actamat.2007.02.032.

[16] S.J. Andersen, C.D. Marioara, R. Vissers, A. Frøseth, H.W. Zandbergen, The structural relation between precipitates in Al–Mg–Si alloys, the Al-matrix and diamond silicon, with emphasis on the trigonal phase U1-MgAl2Si2, Mater. Sci. Eng. A. 444 (2007) 157–169. https://doi.org/10.1016/j.msea.2006.08.084.

[17] M.A. van Huis, J.H. Chen, M.H.F. Sluiter, H.W. Zandbergen, Phase stability and structural features of matrix-embedded hardening precipitates in Al–Mg–Si alloys in the early stages of evolution, Acta Mater. 55 (2007) 2183–2199. https://doi.org/https://doi.org/10.1016/j.actamat.2006.11.019.

[18] S.J. Andersen, C.D. Marioara, A. Frøseth, R. Vissers, H.W. Zandbergen, Crystal structure of the orthorhombic U2-Al4Mg4Si4 precipitate in the Al–Mg–Si alloy system and its relation to the β′ and β″ phases, Mater. Sci. Eng. A. 390 (2005) 127–138. https://doi.org/10.1016/j.msea.2004.09.019.

[19] A.G. Frøseth, R. Høier, P.M. Derlet, S.J. Andersen, C.D. Marioara, Bonding in MgSi and Al-Mg-Si compounds relevant to Al-Mg-Si alloys, Phys. Rev. B. 67 (2003) 224106. https://doi.org/10.1103/PhysRevB.67.224106.

[20] G.A. Edwards, K. Stiller, G.L. Dunlop, M.J. Couper, The precipitation sequence in Al–Mg–Si alloys, Acta Mater. 46 (1998) 3893–3904. https://doi.org/10.1016/S1359-6454(98)00059-7.

[21] G. Sha, H. Möller, W.E. Stumpf, J.H. Xia, G. Govender, S.P. Ringer, Solute nanostructures and their strengthening effects in Al–7Si–0.6Mg alloy F357, Acta Mater. 60 (2012) 692–701. https://doi.org/https://doi.org/10.1016/j.actamat.2011.10.029.

[22] S. Wenner, C.D. Marioara, S.J. Andersen, R. Holmestad, Effect of room temperature storage time on precipitation in Al–Mg–Si(–Cu) alloys with different Mg/Si ratios, Int. J. Mater. Res. 103 (2012) 948–954. https://doi.org/10.3139/146.110795.

[23] C.D. Marioara, S.J. Andersen, H.W. Zandbergen, R. Holmestad, The influence of alloy composition on precipitates of the Al-Mg-Si system, Metall. Mater. Trans. A. 36 (2005) 691–702. https://doi.org/10.1007/s11661-005-0185-1.

[24] C.. Marioara, S.. Andersen, J. Jansen, H.. Zandbergen, The influence of temperature and storage time at RT on nucleation of the β″ phase in a 6082 Al–Mg–Si alloy, Acta Mater. 51 (2003) 789–796. https://doi.org/10.1016/S1359-6454(02)00470-6.

[25] J. Buha, R.N. Lumley, A.G. Crosky, K. Hono, Secondary precipitation in an Al–Mg–Si–Cu alloy, Acta Mater. 55 (2007) 3015–3024. https://doi.org/https://doi.org/10.1016/j.actamat.2007.01.006.

[26] S. Pogatscher, H. Antrekowitsch, H. Leitner, T. Ebner, P.J. Uggowitzer, Mechanisms controlling the artificial aging of Al–Mg–Si Alloys, Acta Mater. 59 (2011) 3352–3363. https://doi.org/10.1016/j.actamat.2011.02.010.

[27] H.S. Hasting, A.G. Frøseth, S.J. Andersen, R. Vissers, J.C. Walmsley, C.D. Marioara, F. Danoix, W. Lefebvre, R. Holmestad, Composition of β″ precipitates in Al–Mg–Si alloys by atom probe tomography and first principles calculations, J. Appl. Phys. 106 (2009) 123527. https://doi.org/10.1063/1.3269714.

[28] F.J.H. Ehlers, Ab initio interface configuration determination for β″ in Al–Mg–Si: Beyond the constraint of a preserved precipitate stoichiometry, Comput. Mater. Sci. 81 (2014) 617–629. https://doi.org/https://doi.org/10.1016/j.commatsci.2013.08.037.

[29] S. Wenner, L. Jones, C.D. Marioara, R. Holmestad, Atomic-resolution chemical mapping of ordered precipitates in Al alloys using energy-dispersive X-ray spectroscopy, Micron. 96 (2017) 103–111. https://doi.org/https://doi.org/10.1016/j.micron.2017.02.007.

[30] S. Takeshi, M.E. A., W. Sigurd, M.C. D., A.S. J., F. Jesper, M. Kenji, H. Randi, Atomic Structures of Precipitates in Al–Mg–Si Alloys with Small Additions of Other Elements, Adv. Eng. Mater. 0 (2018). https://doi.org/10.1002/adem.201800125.

[31] F. De Geuser, W. Lefebvre, D. Blavette, 3D atom probe study of solute atoms clustering during natural ageing and pre-ageing of an Al-Mg-Si alloy, Philos. Mag. Lett. 86 (2006) 227–234. https://doi.org/10.1080/09500830600643270.

[32] J.D. Bryant, The effects of preaging treatments on aging kinetics and mechanical properties in AA6111 aluminum autobody sheet, Metall. Mater. Trans. A. 30 (1999) 1999–2006. https://doi.org/10.1007/s11661-999-0010-3.

[33] R.K.W. Marceau, A. de Vaucorbeil, G. Sha, S.P. Ringer, W.J. Poole, Analysis of strengthening in AA6111 during the early stages of aging: Atom probe tomography and yield stress modelling, Acta Mater. 61 (2013) 7285–7303. https://doi.org/https://doi.org/10.1016/j.actamat.2013.08.033.

[34] S. Pogatscher, H. Antrekowitsch, H. Leitner, D. Pöschmann, Z.L. Zhang, P.J. Uggowitzer, Influence of interrupted quenching on artificial aging of Al–Mg–Si alloys, Acta Mater. 60 (2012) 4496–4505. https://doi.org/https://doi.org/10.1016/j.actamat.2012.04.026.

[35] S. Pogatscher, E. Kozeschnik, H. Antrekowitsch, M. Werinos, S.S.A. Gerstl, J.F. Löffler, P.J. Uggowitzer, Process-controlled suppression of natural aging in an Al–Mg–Si alloy, Scr. Mater. 89 (2014) 53–56. https://doi.org/https://doi.org/10.1016/j.scriptamat.2014.06.025.

[36] M. Murayama, K. Hono, S. M, M. Kikuchi, Atom probe studies on the early stages of precipitation in Al–Mg–Si alloys, Mater. Sci. Eng. A. 250 (1998) 127–132. https://doi.org/10.1016/S0921-5093(98)00548-6.

[37] M. Murayama, K. Hono, Pre-precipitate clusters and precipitation processes in Al–Mg–Si alloys, Acta Mater. 47 (1999) 1537–1548. https://doi.org/10.1016/S1359-6454(99)00033-6.

[38] V. Fallah, A. Korinek, N. Ofori-Opoku, B. Raeisinia, M. Gallerneault, N. Provatas, S. Esmaeili, Atomic-scale pathway of early-stage precipitation in Al–Mg–Si alloys, Acta Mater. 82 (2015) 457–467. https://doi.org/10.1016/j.actamat.2014.09.004.

[39] M. Murayama, K. Hono, W.F. Miao, D.E. Laughlin, The effect of Cu additions on the precipitation kinetics in an Al-Mg-Si alloy with excess Si, Metall. Mater. Trans. A. 32 (2001) 239–246. https://doi.org/10.1007/s11661-001-0254-z.

[40] J. Buha, R.N. Lumley, A.G. Crosky, Precipitation and solute distribution in an interrupted-aged Al–Mg–Si–Cu alloy, Philos. Mag. 88 (2008) 373–390. https://doi.org/10.1080/14786430701847949.

[41] A.I. Morley, M.W. Zandbergen, A. Cerezo, G.D.W. Smith, The Effect of Pre-Ageing and Addition of Copper on the Precipitation Behaviour in Al-Mg-Si Alloys, Mater. Sci. Forum. 519–521 (2006) 543–548. https://doi.org/10.4028/www.scientific.net/MSF.519-521.543.

[42] D.J. Chakrabarti, D.E. Laughlin, Phase relations and precipitation in Al–Mg–Si alloys with Cu additions, Prog. Mater. Sci. 49 (2004) 389–410. https://doi.org/https://doi.org/10.1016/S0079-6425(03)00031-8.

[43] S. Esmaeili, D. Vaumousse, M.W. Zandbergen, W.J. Poole, A. Cerezo, D.J. Lloyd, A study on the early-stage decomposition in the Al–Mg–Si–Cu alloy AA6111 by electrical resistivity and three-dimensional atom probe, Philos. Mag. 87 (2007) 3797–3816. https://doi.org/10.1080/14786430701408312.

[44] K. Matsuda, S. Ikeno, Y. Uetani, T. Sato, Metastable phases in an Al-Mg-Si alloy containing copper, Metall. Mater. Trans. A. 32 (2001) 1293–1299. https://doi.org/10.1007/s11661-001-0219-2.

[45] D. Vaumousse, A. Cerezo, P.J. Warren, S.A. Court, An Atom Probe Study of Fine Scale Structure in AlMgSi(Cu) Alloys, Mater. Sci. Forum. 396–402 (2002) 693–698. https://doi.org/10.4028/www.scientific.net/MSF.396-402.693.

[46] M.W. Zandbergen, A. Cerezo, G.D.W. Smith, Study of precipitation in Al–Mg–Si Alloys by atom probe tomography II. Influence of Cu additions, Acta Mater. 101 (2015) 149–158. https://doi.org/10.1016/j.actamat.2015.08.018.

[47] T. Saito, C.D. Marioara, S.J. Andersen, W. Lefebvre, R. Holmestad, Aberration-corrected HAADF-STEM investigations of precipitate structures in Al–Mg–Si alloys with low Cu additions, Philos. Mag. 94 (2014) 520–531. https://doi.org/10.1080/14786435.2013.857051.

[48] K. Li, A. Béché, M. Song, G. Sha, X. Lu, K. Zhang, Y. Du, S.P. Ringer, D. Schryvers, Atomistic structure of Cu-containing β″ precipitates in an Al–Mg–Si–Cu alloy, Scr. Mater. 75 (2014) 86–89. https://doi.org/https://doi.org/10.1016/j.scriptamat.2013.11.030.

[49] E.A. Mørtsell, C.D. Marioara, S.J. Andersen, I.G. Ringdalen, J. Friis, S. Wenner, J. Røyset, O. Reiso, R. Holmestad, The effects and behaviour of Li and Cu alloying agents in lean Al-Mg-Si alloys, J. Alloys Compd. 699 (2017) 235–242. https://doi.org/https://doi.org/10.1016/j.jallcom.2016.12.273.

[50] Y. Koshino, M. Kozuka, S. Hirosawa, Y. Aruga, Comparative and complementary characterization of precipitate microstructures in Al–Mg–Si(–Li) alloys by transmission electron microscopy, energy dispersive X-ray spectroscopy and atom probe tomography, J. Alloys Compd. 622 (2015) 765–770. https://doi.org/https://doi.org/10.1016/j.jallcom.2014.10.199.

[51] C.D. Marioara, J. Nakamura, K. Matsuda, S.J. Andersen, R. Holmestad, T. Sato, T. Kawabata, S. Ikeno, HAADF-STEM study of β′-type precipitates in an over-aged Al–Mg–Si–Ag alloy, Philos. Mag. 92 (2012) 1149–1158. https://doi.org/10.1080/14786435.2011.642319.

[52] E.A. Mørtsell, C.D. Marioara, S.J. Andersen, J. Røyset, O. Reiso, R. Holmestad, Effects of Germanium, Copper, and Silver Substitutions on Hardness and Microstructure in Lean Al-Mg-Si Alloys, Metall. Mater. Trans. A. 46 (2015) 4369–4379. https://doi.org/10.1007/s11661-015-3039-5.

[53] E.A. Mørtsell, S.J. Andersen, J. Friis, C.D. Marioara, R. Holmestad, Atomistic details of precipitates in lean Al–Mg–Si alloys with trace additions of Ag and Ge studied by HAADF-STEM and DFT, Philos. Mag. 97 (2017) 851–866. https://doi.org/10.1080/14786435.2017.1281461.

[54] T. Saito, F.J.H. Ehlers, W. Lefebvre, D. Hernandez-Maldonado, R. Bjørge, C.D. Marioara, S.J. Andersen, R. Holmestad, HAADF-STEM and DFT investigations of the Zn-containing β″ phase in Al–Mg–Si alloys, Acta Mater. 78 (2014) 245–253. https://doi.org/10.1016/j.actamat.2014.06.055.

[55] T. Saito, S. Wenner, E. Osmundsen, C.D. Marioara, S.J. Andersen, J. Røyset, W. Lefebvre, R. Holmestad, The effect of Zn on precipitation in Al–Mg–Si alloys, Philos. Mag. 94 (2014) 2410–2425. https://doi.org/10.1080/14786435.2014.913819.

[56] L. Ding, Z. Jia, J. Nie, Y. Weng, L. Cao, H. Chen, X. Wu, Q. Liu, The structural and compositional evolution of precipitates in Al-Mg-Si-Cu alloy, Acta Mater. 145 (2018) 437–450. https://doi.org/https://doi.org/10.1016/j.actamat.2017.12.036.

[57] C. Cayron, P.A. Buffat, Transmission electron microscopy study of the β' phase (Al–Mg–Si alloys) and QC phase (Al–Cu–Mg–Si alloys): ordering mechanism and crystallographic structure, Acta Mater. 48 (2000) 2639–2653. https://doi.org/https://doi.org/10.1016/S1359-6454(00)00057-4.

[58] C. Cayron, L. Sagalowicz, O. Beffort, P.A. Buffat, Structural phase transition in Al-Cu-Mg-Si alloys by transmission electron microscopy study on an Al-4 wt% Cu-1 wt% Mg-Ag alloy reinforced by SiC particles, Philos. Mag. A. 79 (1999) 2833–2851. https://doi.org/10.1080/01418619908212027.

[59] L. Arnberg, B. Aurivillius, E. Wahlström, G. Malmros, J. Sjöblom, T.G. Strand, V.F. Sukhoverkhov, The Crystal Structure of Al(x)Cu2Mg(12-x)Si7, (h-AlCuMgSi)., Acta Chem. Scand. 34a (1980) 1–5. https://doi.org/10.3891/acta.chem.scand.34a-0001.

[60] S. Wenner, C.D. Marioara, Q.M. Ramasse, D.-M. Kepaptsoglou, F.S. Hage, R. Holmestad, Atomic-resolution electron energy loss studies of precipitates in an Al–Mg–Si–Cu–Ag alloy, Scr. Mater. 74 (2014) 92–95. https://doi.org/10.1016/j.scriptamat.2013.11.007.

[61] H.K. Hardy, The ageing characteristics of ternary aluminium-copper alloys with cadmium, indium, or tin, J. Inst. Met. 80 (1951) 483.

[62] B. Noble, Theta-prime precipitation in aluminium-copper-cadmium alloys, Acta Metall. 16 (1968) 393–401. https://doi.org/10.1016/0001-6160(68)90026-6.

[63] S.P. Ringer, K. Hono, T. Sakurai, The effect of trace additions of sn on precipitation in Al-Cu alloys: An atom probe field ion microscopy study, Metall. Mater. Trans. A. 26 (1995) 2207–2217. https://doi.org/10.1007/BF02671236.

[64] J.M. Silcock, H.M. Flower, Comments on a comparison of early and recent work on the effect of trace additions of Cd, In, or Sn on nucleation and growth of θ' in Al–Cu alloys, Scr. Mater. 46 (2002) 389–394. https://doi.org/10.1016/S1359-6462(02)00003-9.

[65] L. Bourgeois, C. Dwyer, M. Weyland, J.-F. Nie, B.C. Muddle, The magic thicknesses of θ' precipitates in Sn-microalloyed Al–Cu, Acta Mater. 60 (2012) 633–644. https://doi.org/10.1016/j.actamat.2011.10.015.

[66] L. Bourgeois, J.F. Nie, B.C. Muddle, Assisted nucleation of θ' phase in Al–Cu–Sn: the modified crystallography of tin precipitates, Philos. Mag. 85 (2005) 3487–3509. https://doi.org/10.1080/14786430500228473.

[67] E. Holmes, B. Noble, Resistivity examination of artficial ageing in an aluminium-copper-cadmium alloy, J. Inst. Met. 95 (1967) 106–110.

[68] J.D. Boyd, R.B. Nicholson, A calorimetric determination of precipitate interfacial energies in two Al-Cu alloys, Acta Metall. 19 (1971) 1101–1109. https://doi.org/10.1016/0001-6160(71)90042-3.

[69] R. Sankaran, C. Laird, Effect of trace additions Cd, In and Sn on the interfacial structure and kinetics of growth of θ' plates in Al-Cu alloy, Mater. Sci. Eng. 14 (1974) 271–279. https://doi.org/10.1016/0025-5416(74)90108-6.

[70] J.M. Silcock, Intermediate precipitates in aged binary alloys of aluminium with cadmium, indium and tin, J. Inst. Met. 84 (1955) 19.

[71] T. Homma, M.P. Moody, D.W. Saxey, S.P. Ringer, Effect of Sn Addition in Preprecipitation Stage in Al-Cu Alloys: A Correlative Transmission Electron Microscopy and Atom Probe Tomography Study, Metall. Mater. Trans. A. 43 (2012) 2192–2202. https://doi.org/10.1007/s11661-012-1111-y.

[72] M. Werinos, H. Antrekowitsch, T. Ebner, R. Prillhofer, P.J. Uggowitzer, S. Pogatscher, Hardening of Al–Mg–Si alloys: Effect of trace elements and prolonged natural aging, Mater. Des. 107 (2016) 257–268. https://doi.org/10.1016/j.matdes.2016.06.014.

[73] M. Werinos, H. Antrekowitsch, T. Ebner, R. Prillhofer, W.A. Curtin, P.J. Uggowitzer, S. Pogatscher, Design strategy for controlled natural aging in Al–Mg–Si alloys, Acta Mater. 118 (2016) 296–305. https://doi.org/10.1016/j.actamat.2016.07.048.

[74] M.F. Francis, W.A. Curtin, Microalloying for the controllable delay of precipitate formation in metal alloys, Acta Mater. 106 (2016) 117–128. https://doi.org/10.1016/j.actamat.2016.01.014.

[75] F. Qian, E.A. Mørtsell, C.D. Marioara, S.J. Andersen, Y. Li, Improving ageing kinetics and precipitation hardening in an Al-Mg-Si alloy by minor Cd addition, Materialia. 4 (2018) 33–37. https://doi.org/https://doi.org/10.1016/j.mtla.2018.09.006.

[76] S.J. Andersen, Quantification of the Mg2Si β″ and β' phases in AlMgSi alloys by transmission electron microscopy, Metall. Mater. Trans. A. 26 (1995) 1931–1937. https://doi.org/10.1007/BF02670664.

[77] F. Qian, S. Jin, G. Sha, Y. Li, Enhanced dispersoid precipitation and dispersion strengthening in an Al alloy by microalloying with Cd, Acta Mater. 157 (2018) 114–125. https://doi.org/https://doi.org/10.1016/j.actamat.2018.07.001.

[78] D. Vaumousse, A. Cerezo, P.J. Warren, A procedure for quantification of precipitate microstructures from three-dimensional atom probe data, Ultramicroscopy. 95 (2003) 215–221. https://doi.org/https://doi.org/10.1016/S0304-3991(02)00319-4.

[79] G. Kresse, J. Furthmüller, Efficiency of ab-initio total energy calculations for metals and semiconductors using a plane-wave basis set, Comput. Mater. Sci. 6 (1996) 15–50. https://doi.org/https://doi.org/10.1016/0927-0256(96)00008-0.

[80] P.E. Blöchl, Projector augmented-wave method, Phys. Rev. B. 50 (1994) 17953–17979. https://link.aps.org/doi/10.1103/PhysRevB.50.17953.

[81] J.P. Perdew, K. Burke, M. Ernzerhof, Generalized Gradient Approximation Made Simple, Phys. Rev. Lett. 77 (1996) 3865–3868. https://doi.org/10.1103/PhysRevLett.77.3865.

[82] H.J. Monkhorst, J.D. Pack, Special points for Brillouin-zone integrations, Phys. Rev. B. 13 (1976) 5188–5192. https://link.aps.org/doi/10.1103/PhysRevB.13.5188.

[83] P.E. Blöchl, O. Jepsen, O.K. Andersen, Improved tetrahedron method for Brillouin-zone integrations, Phys. Rev. B. 49 (1994) 16223–16233. https://link.aps.org/doi/10.1103/PhysRevB.49.16223.

[84] D. Zhao, O.M. Løvvik, K. Marthinsen, Y. Li, Impurity effect of Mg on the generalized planar fault energy of Al, J. Mater. Sci. 51 (2016) 6552–6568. https://doi.org/10.1007/s10853-016-9834-6.

[85] D. Zhao, O.M. Løvvik, K. Marthinsen, Y. Li, Combined effect of Mg and vacancy on the generalized planar fault energy of Al, J. Alloys Compd. 690 (2017) 841–850. https://doi.org/https://doi.org/10.1016/j.jallcom.2016.08.203.

[86] Y. Du, Y.. Chang, B. Huang, W. Gong, Z. Jin, H. Xu, Z. Yuan, Y. Liu, Y. He, F.-Y. Xie, Diffusion coefficients of some solutes in fcc and liquid Al: critical evaluation and correlation, Mater. Sci. Eng. A. 363 (2003) 140–151. https://doi.org/10.1016/S0921-5093(03)00624-5.

[87] V. Fallah, B. Langelier, N. Ofori-Opoku, B. Raeisinia, N. Provatas, S. Esmaeili, Cluster evolution mechanisms during aging in Al–Mg–Si alloys, Acta Mater. 103 (2016) 290–300. https://doi.org/https://doi.org/10.1016/j.actamat.2015.09.027.

[88] A. Serizawa, T. Sato, W.J. Poole, The characterization of dislocation–nanocluster interactions in Al–Mg–Si(–Cu/Ag) alloys, Philos. Mag. Lett. 90 (2010) 279–287. https://doi.org/10.1080/09500831003633231.

[89] M. Torsæter, W. Lefebvre, S.J. Andersen, C.D. Marioara, J.C. Walmsley, R. Holmestad, Clustering Behaviour in Al-Mg-Si Alloys Investigated by APT, in: Proc. 12th Int. Conf. Alum. Alloy., Yokohama, Japan, 2010: p. 1385.

[90] A. Serizawa, S. Hirosawa, T. Sato, Three-Dimensional Atom Probe Characterization of Nanoclusters Responsible for Multistep Aging Behavior of an Al-Mg-Si Alloy, Metall. Mater. Trans. A. 39 (2008) 243–251. https://doi.org/10.1007/s11661-007-9438-5.

[91] S. Pogatscher, H. Antrekowitsch, H. Leitner, A.S. Sologubenko, P.J. Uggowitzer, Influence of the thermal route on the peak-aged microstructures in an Al–Mg–Si aluminum alloy, Scr. Mater. 68 (2013) 158–161. https://doi.org/https://doi.org/10.1016/j.scriptamat.2012.10.006.

[92] C. Liu, P. Ma, L. Zhan, M. Huang, J. Li, Solute Sn-induced formation of composite β′/β″ precipitates in Al-Mg-Si alloy, Scr. Mater. 155 (2018) 68–72. https://doi.org/https://doi.org/10.1016/j.scriptamat.2018.06.028.

[93] C. Wolverton, Solute–vacancy binding in aluminum, Acta Mater. 55 (2007) 5867–5872. https://doi.org/10.1016/j.actamat.2007.06.039.

[94] Thermodynamic database, TCAL4-TCS Al-based alloy database, Version 4.0, Thermo-Calc software, (n.d.). www.thermocalc.com.

[95] D. Zhao, F. Qian, S. Jin, C.D. Marioara, S.J. Andersen, G. Sha, Y. Li, Atomic-scale revisiting the stimulated age-hardening in Al-Cu alloy with Cd trace addition, To Be Submitt. (2020).